Hinkkanen, Marko; Luomi, Jorma

Zero-speed operation of sensorless induction motors using full-order flux observer

Published in:
Nordic Workshop on Power and Industrial Electronics (NORPIE/2002)

Published: 12/08/2002

Document Version
Peer-reviewed accepted author manuscript, also known as Final accepted manuscript or Post-print

Please cite the original version:
Hinkkanen, M., & Luomi, J. (2002). Zero-speed operation of sensorless induction motors using full-order flux observer. In *Nordic Workshop on Power and Industrial Electronics (NORPIE/2002)*

Zero-Speed Operation of Sensorless Induction Motors Using Full-Order Flux Observer

Marko Hinkkanen and Jorma Luomi

***Abstract*— This paper deals with the flux estimation for sensorless induction motor drives. Stable zero-speed operation is achieved by using a speed-adaptive full-order flux observer and a simple software compensation of inverter nonlinearities. No voltage feedback is needed for the compensation and hardware costs can be lowered. Experimental results including stable zero-speed operation are shown.**

***Index Terms*— Induction machines, AC motor drives, flux estimation.**

I. Introduction

Speed-sensorless induction motor drives have developed outstandingly during the last years. Nonetheless, very-low-speed operation of general-purpose induction motors is still a challenge.

Several flux estimators for speed-sensorless drives have been proposed; the most promising ones are the voltage model [1], the speed-adaptive full-order flux observer [2], [3], and their modifications. Full-order flux observers offer good performance and robustness against parameter errors and measurement noise. A disadvantage is a small instable region in the regeneration mode at low speeds [4]–[6]. Very-low-speed and zero-speed operation using a full-order observer was attained in [7], where measurement of the stator voltage was used. Furthermore, calculation of the stator dynamics was implemented by using analogue integrators.

The voltage model is simpler than the full-order flux observer but several disadvantages exist: drift problems; sensitivity to the stator resistance estimate at low speeds; and the need for initial conditions. However, very-low-speed operation was successfully achieved in [8] by using a modified voltage model flux estimator, where dead-time compensation based on voltage feedback was used.

Voltage-source inverters employing pulse width modulation introduce a nonlinear voltage gain. The inverter nonlinearities, mainly caused by the dead-time effect and power device voltage drops, are substantial at low speeds. Unless the stator voltage is measured, the nonlinearities should be compensated in order to operate the sensorless drive at very low speeds, no matter which flux estimator is chosen. Some of the proposed dead-time compensation methods require the measurement of the phase voltage change instants [9] whereas others only need the current measurement [10]–[12]. The compensation for power device voltage drops is based on the measured current [8], [10]–[12].

Very-low-speed operation is desirable for most general-purpose drives but, on the other hand, hardware costs should be as low as possible. This paper demonstrates the zero-speed and very-low-speed operation of the sensorless drive using a low-cost compensation for inverter nonlinearities. Potential-free measurement of the change instants of the inverter output voltages is not needed, and the hardware costs can thus be lowered. Distortion due to the slightly incomplete compensation is overcome by using the speed-adaptive full-order flux observer offering robustness against measurement noise. Furthermore, the start-up is simpler than that of the voltage model since no initial condition of the flux is needed.

In the following, the induction motor model and the flux observer are first defined. Then, the adopted compensation method for the inverter nonlinearities is described. Finally, the control system based on the rotor flux orientation is introduced and the experimental results are presented.

II. Induction Motor Model

The parameters of the dynamic Γ-equivalent circuit of an induction motor are the stator resistance R_s, the rotor resistance R_R, the stator transient inductance L'_s, and the magnetizing inductance L_M. The angular speed of the rotor is denoted by ω_m, the angular speed of the reference frame ω_k, the stator current space vector $\underline{i}_s$, and the stator voltage $\underline{u}_s$. When the stator flux $\underline{\psi}_s$ and the rotor flux $\underline{\psi}_R$ are chosen as state variables, the state-space representation of the induction motor becomes

$$\dot{\underline{\mathbf{x}}} = \underbrace{\begin{bmatrix} -\frac{1}{\tau'_s} - j\omega_k & \frac{1}{\tau'_s} \\ \frac{1-\sigma}{\tau'_r} & -\frac{1}{\tau'_r} - j\left(\omega_k - \omega_m\right) \end{bmatrix}}_{\mathbf{A}} \underline{\mathbf{x}} + \underbrace{\begin{bmatrix} 1 \\ 0 \end{bmatrix}}_{\mathbf{B}} \underline{u}_s \quad (1a)$$

$$\underline{i}_s = \underbrace{\begin{bmatrix} \frac{1}{L'_s} & -\frac{1}{L'_s} \end{bmatrix}}_{\mathbf{C}} \underline{\mathbf{x}} \quad (1b)$$

where the state vector is $\underline{\mathbf{x}} = [\underline{\psi}_s \quad \underline{\psi}_R]^T$, and the parameters expressed in terms of the Γ-equivalent circuit parameters are $\sigma = L'_s/(L_M + L'_s)$, $\tau'_s = L'_s/R_s$, and $\tau'_r = \sigma L_M/R_R$.

The authors are with the Power Electronics Laboratory, Helsinki University of Technology, P.O. Box 3000, FIN-02015 HUT, Finland (e-mail: marko.hinkkanen@hut.fi; jorma.luomi@hut.fi).

III. Speed-Adaptive Full-Order Flux Observer

Conventionally, the stator current and the rotor flux are used as state variables in full-order flux observers. However, choosing the stator and rotor fluxes as state variables is preferred since a simple digital implementation having small discretization errors can then be exploited [13]. In addition, the observer could be used with stator flux oriented control or direct torque control [14] as well as with rotor flux oriented control.

The full-order flux observer using the fluxes as state variables is defined by

$$\dot{\hat{\underline{\mathbf{x}}}} = \hat{\underline{\mathbf{A}}}\,\hat{\underline{\mathbf{x}}} + \mathbf{B}\underline{u}_s + \underline{\mathbf{L}}(\underline{i}_s - \hat{\underline{i}}_s) \tag{2a}$$

$$\hat{\underline{i}}_s = \mathbf{C}\hat{\underline{\mathbf{x}}} \tag{2b}$$

where the observer state vector is $\hat{\underline{\mathbf{x}}} = [\hat{\underline{\psi}}_s \quad \hat{\underline{\psi}}_R]^T$, the observer gain $\underline{\mathbf{L}} = [\underline{l}_s \quad \underline{l}_r]^T$, and the system matrix

$$\hat{\underline{\mathbf{A}}} = \begin{bmatrix} -\frac{1}{\tau_s'} - j\omega_k & \frac{1}{\tau_s'} \\ \frac{1-\sigma}{\tau_r'} & -\frac{1}{\tau_r'} - j(\omega_k - \hat{\omega}_m) \end{bmatrix} \tag{2c}$$

where the estimate is marked by the symbol $\hat{}$. The conventional speed adaptation law is

$$\begin{aligned} \hat{\omega}_m = &-\gamma_p \operatorname{Im}\left\{(\underline{i}_s - \hat{\underline{i}}_s)\hat{\underline{\psi}}_R^*\right\} \\ &- \gamma_i \int \operatorname{Im}\left\{(\underline{i}_s - \hat{\underline{i}}_s)\hat{\underline{\psi}}_R^*\right\} dt \end{aligned} \tag{3}$$

where γ_p and γ_i are the adaptation gains and the complex conjugates are marked by the symbol *. The adaptation law (3) is often derived based on the Lyapunov stability theorem [2] or the Popov hyperstability theorem [3]. However, the adaptation law is not guaranteed to be globally stable since approximations regarding unknown states have been used or the positive-realness condition is not satisfied. Actually, it is well known that there is a small instable region in the regeneration mode at low speeds [4]–[6]. The size of the region could be reduced by choosing $\underline{\mathbf{L}}$ suitably. For simplicity, $\underline{\mathbf{L}} = 0$ is chosen in this paper.

IV. Compensation for Inverter Nonlinearities

The effect of inverter nonlinearities on the stator voltage is substantial at low speeds. The simple software compensation approach requiring only the current measurement [10]–[12] is adopted and shortly reviewed in the following.

A. Dead Time and Power Device Voltage Drops

The most significant nonlinearity is the dead-time effect. In order to prevent the shoot-through of the dc link, a small lock-out time is introduced by the inverter control. The actual dead time T_d is the lock-out time plus device turn-on time minus device turn-off time [12].

Another important nonlinearity is caused by the power device voltage drops. To simplify the following analysis, active switches and freewheeling diodes are assumed to have identical voltage drop characteristics modelled by the threshold voltage u_{th} and the on-state slope resistance R_d.

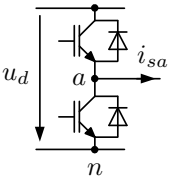

Fig. 1. Inverter leg of phase a.

The voltage of the a-phase with respect to the negative dc bus (Fig. 1) averaged over one switching period T_{sw} can be expressed as

$$u_{san} = u_{san,ref} \underbrace{-\frac{T_d}{T_{sw}} u_d \operatorname{sign}(i_{sa})}_{\text{dead-time effect}} \underbrace{-u_{th}\operatorname{sign}(i_{sa}) - R_d i_{sa}}_{\text{power device voltage drop}} \tag{4}$$

where the ideal voltage is $u_{san,ref}$, the dc-link voltage u_d, and the switching frequency $f_{sw} = 1/T_{sw}$. Since the voltages of the phases b and c can be expressed similarly, the stator voltage space vector becomes [8], [15]

$$\underline{u}_s = \underline{u}_{s,ref} - \underbrace{\left(\frac{T_d}{T_{sw}} u_d + u_{th}\right)\operatorname{sig}(\underline{i}_s)}_{\Delta\underline{u}} - R_d\underline{i}_s \tag{5}$$

where $\underline{u}_{s,ref}$ is the reference voltage and

$$\operatorname{sig}(\underline{i}_s) = \frac{2}{3}\left[\operatorname{sign}(i_{sa}) + \operatorname{sign}(i_{sb})e^{j\frac{2\pi}{3}} + \operatorname{sign}(i_{sc})e^{j\frac{4\pi}{3}}\right] \tag{6}$$

is a nonlinear function having an amplitude of 4/3.

B. Compensation

The compensation is carried out in a feedforward manner. The compensated reference voltage for the PWM is

$$\underline{u}_{s,ref}^c = \underline{u}_{s,ref} + \Delta\hat{\underline{u}} \tag{7}$$

The amplitude of $\Delta\hat{\underline{u}}$ can be obtained based on manufacturer specifications of the power devices, experimental data, or by using off-line identification methods, e.g., [11]. Since the amplitude of $\Delta\hat{\underline{u}}$ depends on temperature and current level, a look-up table could be used to adjust it on line [12]. The effect of the resistance R_d is taken into account by adding its estimate to the stator resistance estimate, i.e., $R_s^c = R_s + R_d$ is used in the flux observer.

Fig. 2 shows an example of the current and reference voltage waveforms without dead-time compensation obtained using the experimental setup described in Section VI. The current was regulated to have a frequency of 0.25 Hz and an amplitude of 1.0 A. The reference voltage was the output of the current controller. Since the current is sinusoidal and the machine is symmetric, the actual stator voltage should also be sinusoidal. By using this fact, the distortion voltage $\Delta\underline{u}$ shown in Fig. 2 was calculated.

Fig. 3 shows the measured current and reference voltage waveforms when the dead-time compensation is used. The amplitude of $\Delta\hat{\underline{u}}$ was obtained based on Fig. 2. It can

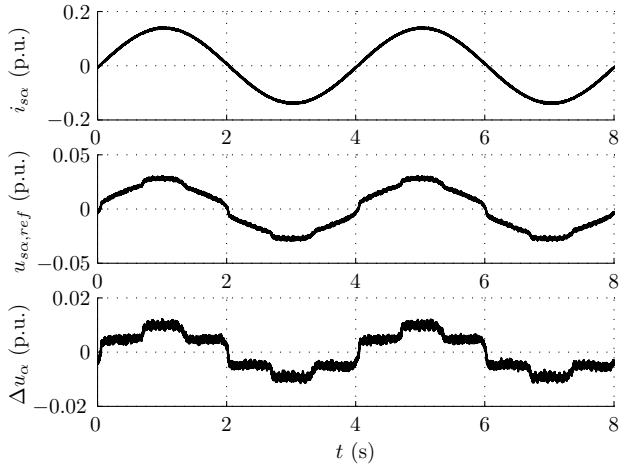

Fig. 2. No compensation of inverter nonlinearities. The first subplot shows the real component of the measured regulated stator current having a frequency of 0.005 p.u. The second subplot shows the real component of the reference voltage. The third subplot presents the real component of the calculated distortion voltage.

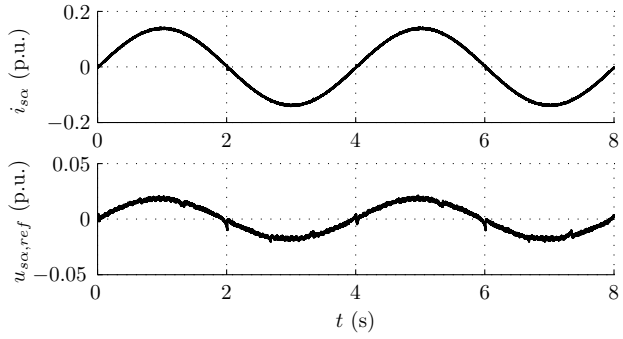

Fig. 3. Compensation of inverter nonlinearities. The first subplot shows the measured regulated stator current having a frequency of 0.005 p.u. The second subplot shows the reference voltage.

be seen that the compensation is incomplete near phase current zero crossings. Spikes in the reference voltage are due to a change of the current direction during the dead time, which causes the zero current clamping phenomenon. To eliminate the spikes, it would be possible to carry out the compensation as presented in [16].

V. Control System

The full-order flux observer and the compensation of inverter nonlinearities were investigated experimentally. The control was based on the direct rotor flux orientation and synchronous-frame current control [17]. The overall block diagram of the system is shown in Fig. 4.

The speed and flux controllers were conventional PI-controllers. The bandwidths of the controllers are given in Table I. Fairly high flux and speed controller bandwidths can be chosen since the output of the flux observer is smooth. The speed adaptation gains were $\gamma_p = 10$ and $\gamma_i = 10000$.

The sampling was synchronized to the modulation, and both the switching frequency and the sampling frequency were 5 kHz. The dc-link voltage was measured, and the

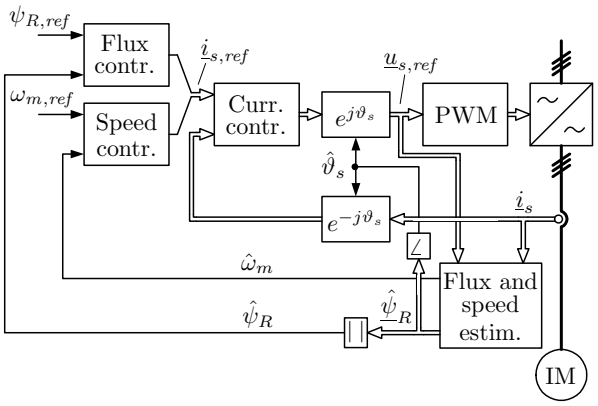

Fig. 4. The direct rotor flux oriented controller. The electrical variables shown on the left hand side of the coordinate transformations are in the (estimated) rotor flux reference frame and the variables on the right hand side are in the stator reference frame. The block "PWM" includes the compensation for inverter nonlinearities.

TABLE I
Bandwidths, Base Value $2\pi \cdot 50$ Hz.

Current control	$\alpha_c = 8$ p.u.
Speed control	$\alpha_s = 0.04\alpha_c$
Flux control	$\alpha_f = \alpha_s$

reference stator voltage obtained from the current controller was used for the flux observer. Inverter nonlinearities were compensated according to (7). The zero current clamping phenomenon was not compensated which can be seen in the following experimental results.

VI. Experimental Results

The experimental setup is shown in Fig. 5. A 2.2-kW four-pole induction motor (Table II) was fed by a frequency converter controlled by a dSpace DS1103 PPC/DSP board. The base values used in figures are: angular frequency $2\pi \cdot 50$ s^{-1}, current $\sqrt{2} \cdot 5.0$ A, and flux 1.0 Wb.

An experimental result showing zero-speed operation during a rated-load torque step is shown in Fig. 6. The speed reference was set to a frequency of 0 Hz. The rated-load torque step was applied at $t = 2$ s, and the load torque was removed at $t = 8$ s. It can be seen that both the flux and the speed are correctly observed. After removing the load, the flux is still properly estimated and the load torque could be applied again.

Fig. 7 demonstrates an experiment similar to that of Fig. 6 but now one third of the rated-load torque step was applied and the load torque was removed at $t = 10$ s. Again, the system behaves stably. A small speed error can be seen when the load torque is applied, which is mainly caused by the inaccurate motor parameters in the flux observer. When the stator frequency is small (i.e., the load torque is light in this experiment), the speed and flux estimation becomes more sensitive to inaccurate motor parameters and measurement noise. This is a well-known property of most sensorless flux estimators based on the

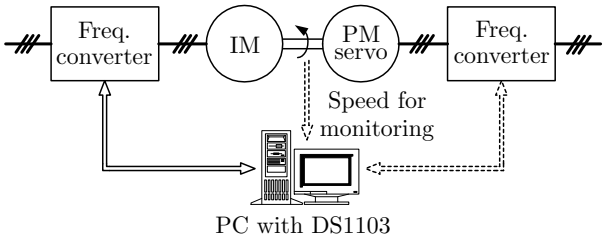

Fig. 5. The experimental setup. The PM servo motor was used as the loading machine.

TABLE II
PARAMETERS FOR THE 2.2-KW FOUR-POLE 400-V 50-HZ MOTOR.

Stator resistance R_s	3.67 Ω
Rotor resistance R_R	2.10 Ω
Magnetizing inductance L_M	0.224 H
Stator transient inductance L'_s	0.0209 H
Moment of inertia J_{tot}	0.0155 kgm^2
Rated speed	1430 r/min
Rated current	5.0 A
Rated torque	14.6 Nm

fundamental model of the motor. Under no load, however, the zero stator frequency is not problem when using the speed-adaptive full-order flux observer.

An experimental result of very-low-speed no-load operation is presented in Fig. 8. In this experiment, only about 2/3 of the distortion voltage $\Delta\underline{\hat{u}}$ was compensated in order to reduce the reference voltage spikes due to the zero current clamping. The speed reference was initially set to a frequency of −0.25 Hz and a speed reversal to the frequency of 0.25 Hz was applied at $t = 5$ s. The average speed is well regulated but the content of the sixth harmonic in the estimated and actual speed is fairly high, which is caused by the incomplete dead-time compensation. Since the distorted speed estimate is the input of the speed controller, the sixth harmonic is also found in the q-component of the reference current (and thus in the actual current and finally in the actual speed). However, the results are very good in spite of incomplete compensation of inverter nonlinearities.

VII. Conclusions

This paper has demonstrated that speed-sensorless very-low-speed operation of an induction motor is possible using low-cost compensation of inverter nonlinearities. Distortion due to the slightly incomplete compensation can be overcome by using the speed-adaptive full-order flux observer offering robustness against measurement noise. However, if the ripple content of the torque at very low speeds is an important issue, the zero current clamping phenomenon should be compensated or the voltage-feedback type dead-time compensation should be used. Future research is needed to solve the instability problem in the regeneration mode at low speeds.

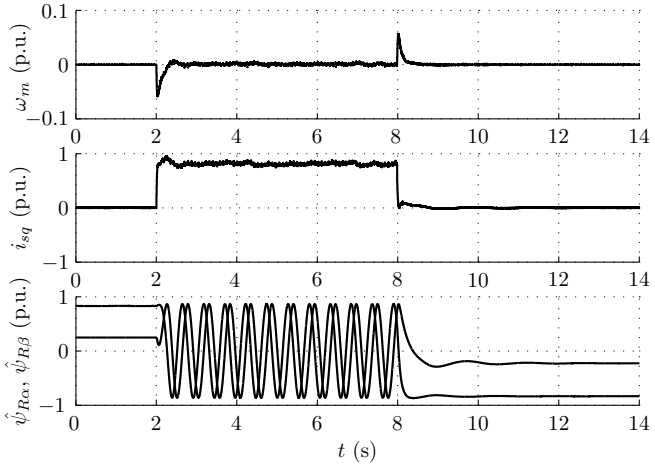

Fig. 6. Experimental results showing the zero-speed operation when a rated-load torque step is applied. The speed reference was set to zero. The first subplot shows the measured speed and the estimated speed. The second subplot shows the q-component of the stator current in the estimated rotor flux reference frame. The third subplot presents the real and imaginary parts of the estimated rotor flux in the stator reference frame.

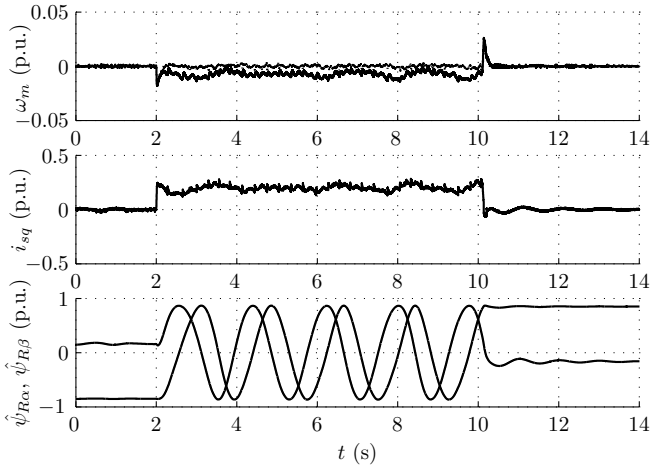

Fig. 7. Experimental results showing zero-speed operation when one third of the rated-load torque step is applied. Explanations of the curves are as in Fig. 6 (the actual speed is the lower curve).

References

[1] X. Xu and D.W. Novotny, "Implementation of direct stator flux orientation control on a versatile DSP based system," *IEEE Transactions on Industry Applications*, vol. 27, no. 4, pp. 694–700, July/Aug. 1991.

[2] H. Kubota, K. Matsuse, and T. Nakano, "DSP-based speed adaptive flux observer of induction motor," *IEEE Transactions on Industry Applications*, vol. 29, no. 2, pp. 344–348, Mar./Apr. 1993.

[3] G. Yang and T.-H. Chin, "Adaptive-speed identification scheme for a vector-controlled speed sensorless inverter-induction motor drive," *IEEE Transactions on Industry Applications*, vol. 29, no. 4, pp. 820–825, July/Aug. 1993.

[4] S. Suwankawin and S. Sangwongwanich, "Stability analysis and design guidelines for a speed-sensorless induction motor drive," in *Proceedings of the Power Conversion Conference*, Nagaoka, Japan, Aug. 1997, vol. 2, pp. 583–588.

[5] H. Tajima, G. Guidi, and H. Umida, "Consideration about problems and solutions of speed estimation method and parameter tuning for speed sensorless vector control of induction motor drives," in *Conference Record of the IEEE Industry Applications Conference, Thirty-Fifth IAS Annual Meeting*, Rome, Italy, Oct. 2000, vol. 3, pp. 1787–1793.

[6] H. Kubota, I. Sato, Y. Tamura, K. Matsuse, H. Ohta, and

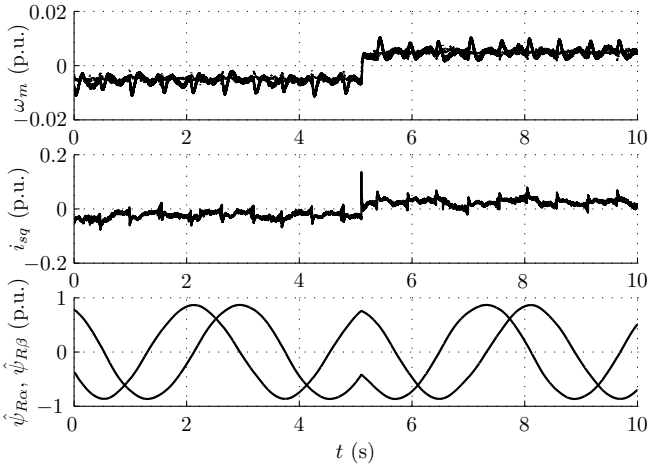

Fig. 8. Experimental results showing the speed reversal from the speed −0.005 p.u. to 0.005 p.u. Explanations of the curves are as in Fig. 6.

Y. Hori, "Stable operation of adaptive observer based sensorless induction motor drives in regenerating mode at low speeds," in *Conference Record of the IEEE Industry Applications Conference, Thirty-Sixth IAS Annual Meeting*, Chicago, IL, Sept./Oct. 2001, vol. 1, pp. 469–474.

[7] B. Peterson, *Induction machine speed estimation – observations on observers*, Ph.D. thesis, Department of Industrial Electrical Engineering and Automation, Lund University, Lund, Sweden, Feb. 1996.

[8] J. Holtz and J. Quan, "Sensorless vector control of induction motors at very low speed using a nonlinear inverter model and parameter identification," in *Conference Record of the IEEE Industry Applications Conference, Thirty-Sixth IAS Annual Meeting*, Chicago, IL, Sept./Oct. 2001, vol. 4, pp. 2614–2621.

[9] Y. Murai, T. Watanabe, and H. Iwasaki, "Waveform distortion and correction circuit for PWM inverters with switching lag-times," *IEEE Transactions on Industry Applications*, vol. IA-23, no. 5, pp. 881–886, Sept./Oct. 1987.

[10] J.K. Pedersen, F. Blaabjerg, J.W. Jensen, and P. Thogersen, "An ideal PWM-VSI inverter with feedforward and feedback compensation," in *Fifth European Conference on Power Electronics and Applications (EPE'93)*, Brighton, U.K., Sept. 1993, vol. 4, pp. 312–318.

[11] J.-W. Choi and S.-K. Sul, "Inverter output voltage synthesis using novel dead time compensation," *IEEE Transactions on Power Electronics*, vol. 11, no. 2, pp. 221–227, Mar. 1996.

[12] A.R. Muñoz-García and T.A. Lipo, "On-line dead-time compensation technique for open-loop PWM-VSI drives," *IEEE Transactions on Power Electronics*, vol. 14, no. 4, pp. 683–689, July 1999.

[13] M. Hinkkanen and J. Luomi, "Novel full-order flux observer structure for speed sensorless induction motors," in *The 27th Annual Conference of the IEEE Industrial Electronics Society (IECON'01)*, Denver, CO, Nov./Dec. 2001, vol. 2, pp. 1333–1338.

[14] J. Maes and J.A. Melkebeek, "Speed-sensorless direct torque control of induction motors using an adaptive flux observer," *IEEE Transactions on Industry Applications*, vol. 36, no. 3, pp. 778–785, May/June 2000.

[15] J. Holtz, "Pulsewidth modulation for electronic power conversion," *Proceedings of the IEEE*, vol. 82, no. 8, pp. 1194–1214, Aug. 1994.

[16] J.-W. Choi and S.-K. Sul, "A new compensation strategy reducing voltage/current distortion in PWM VSI systems operating with low output voltages," *IEEE Transactions on Industry Applications*, vol. 31, no. 5, pp. 1001–1008, Sept./Oct. 1995.

[17] L. Harnefors and H.-P. Nee, "Model-based current control of AC machines using the internal model control method," *IEEE Transactions on Industry Applications*, vol. 34, no. 1, pp. 133–141, Jan./Feb. 1998.